The Abdus Salam
International Centre for Theoretical Physics

EMAS 2008

8th EMAS Regional Workshop on

Electron Probe Microanalysis of Materials Today

Practical Aspects

including a session on

synchrotron-based microanalysis

19 - 22 April 2008

Adriatico Guesthouse
The Abdus Salam International Centre for Theoretical Physics
Trieste, Italy

Book of Abstracts

ELECTRON PROBE MICROANALYSIS OF THIN FILMS AND MULTILAYERS

Xavier Llovet[1]* and C. Merlet[2]

1 *Universitat de Barcelona, Serveis Cientfíco-Tècnics*
C/ Lluís Solé i Sabarís 1-3, ES-08028 Barcelona, Spain
2 *Université de Montpellier II, CNRS, UMR 5243*
Place Eugène Bataillon, FR-34095 Montpellier, France
** xavier@giga.sct.ub.es*

INTRODUCTION

Electron probe microanalysis (EPMA) is a non-destructive analytical technique employed for determining the local composition of solid samples [1, 2]. The technique is based on the measurement of characteristic X-ray intensities emitted by the elements present in the sample when the latter is bombarded with a focused electron beam. For each element, the ratio of the characteristic X-ray intensity emitted from the sample to that emitted from a standard of known composition is measured. This ratio is usually referred to as k-ratio. The transformation from measured k-ratios to concentrations is performed by means of relatively simple, analytical algorithms, which assume that the sample region from which X-rays emerge has a homogeneous composition. For keV electron beams, this region is typically of the order of several micrometres, depending on the density of the material and the analytical conditions. Accordingly, EPMA is suitable for the analysis of samples that are homogeneous at the micrometre scale. The electron microprobe instrument, as well as the basis of quantitative analysis, was developed by Raimond Castaing [3].

Soon after Castaing's development, analyses of thin films by EPMA were reported by several authors who used empirical techniques (see e.g. [4] and references therein) or fitted experimental k-ratios to the results of Monte Carlo (MC) simulations [5]. Later on, EPMA algorithms were extended so as to allow the analysis of thin films and multilayers in a systematic way and the so-called thin-film programmes became available [6 - 10]. Owing to these developments, EPMA has proven to be a versatile tool for thin-film characterisation, supplementing the information obtained from conventional surface-analytical techniques and providing also complementary information about the lateral variation in thickness and composition of thin films at the micrometre scale.

The purpose of this talk is to review the basic principles and procedures of thin film analysis by EPMA, describing in detail one of the thin-film programmes available, *X-FILM* [10], and to provide some examples of applications which illustrate the capabilities of the technique. Extensive reviews of thin-film analysis by EPMA have been published elsewhere [11 - 14].

QUANTITATIVE ANALYSIS

When an electron beam impinges on a sample, electrons interact repeatedly with the sample atoms until they come to rest or emerge from the surface. In some interactions, electrons lose energy by producing a vacancy in an electron shell (ionisation). This vacancy can migrate to outer shells through radiative and non-radiative transitions. When the transition is radiative, the vacancy is filled by an electron from an outer shell and characteristic X-rays are emitted. The probability of radiative transitions is given by the fluorescence yield. X-rays originate at all depths extending from the surface to some maximum depth, which depends on the material and on the energy of incident electrons. Before emerging from the surface, generated X-rays may interact with the sample atoms through different mechanisms, and as a result, fluorescent X-rays may be emitted. The combined effect of all photon interactions is summarized by means of the mass-attenuation coefficient.

Bulk analysis

Consider a homogeneous sample of a given composition (for simplicity we assume that the material is a compound), whose molecular weight is given by $A_\mathrm{M} = \sum a_i A_i$, where a_i is the number of atoms per molecule of element *i*, whose atomic number and atomic weight are Z_i and A_i, respectively. The concentration of element *i*, in terms of the mass fraction, is given by:

$$c_i = \frac{a_i\, A_i}{\sum\limits_j a_j\, A_j} \tag{1}$$

The number of atoms *i* per unit volume is $(N_A\rho/A_i)c_i$, where ρ is the mass density of the material. Let us assume that the sample is irradiated with an electron beam of energy *E*, impinging normally on the sample surface and that characteristic X-rays of element *i* are recorded with an X-ray spectrometer placed at a take-off angle θ. The intensity of a given X-ray line can be evaluated as:

$$I_i = n_\mathrm{el}\, \epsilon\, \frac{\Omega}{4\pi}\, \omega_i\, p_i\, (1 + T_{CK})\, \left[\int_0^\infty \phi_i(z)\, \exp\left(-\mu_i \csc\theta z\right)\, \mathrm{d}z\right]\, \mathcal{F} \tag{2}$$

where n_el is the number of incident electrons, ε is the spectrometer efficiency, $\Omega/4\pi$ is the solid angle of collection, μ/ρ is the mass-attenuation coefficient, ω_i is the fluorescence yield, p_i is the relative intensity of the X-ray line, *F* is a factor that takes into account fluorescence from X-rays (characteristic and bremsstrahlung) generated in the sample [1] and $1 + T_{CK}$ accounts for the enhancement of X-rays due to Coster-Kronig transitions (non-radiative transitions which lead to two vacancies in the same shell). In Eq. (2), $\phi_i(z)$ is the depth-distribution of ionisations, i.e.

$$\int_0^\infty \phi_i(z)\, \mathrm{d}z \tag{3}$$

is the total number of ionisations produced in the sample. Following the pioneering work of Castaing [3], $\phi(z)$ is normalized to the number of ionisations produced per unit thickness in an infinitesimal, self-supporting layer of the element of interest, i.e. $(N_{A}\rho/A_i)\sigma_i(E)$, where $\sigma_i(E)$ is the probability of producing a vacancy in the atomic shell. The new function, referred to as $\Phi(\rho z)$, is dimensionless and it can be measured experimentally in a relatively simple way using the tracer method [3]. The total number of ionisations is given by:

$$\frac{N_{\mathrm{A}}}{A_i}\,\sigma_i(E)\int_0^{\infty}\Phi(\rho z)\,\mathrm{d}\rho z \tag{4}$$

Replacing $\phi(\rho z)$ by $\Phi(\rho z)$ in Eq. (2), the emitted X-ray intensity can be written as:

$$I_i = \mathcal{A}\,c_i\,\left[\int_0^{\infty}\Phi_i(\rho z)\;\exp\left(-\chi_i\,\rho z\right)\;\mathrm{d}(\rho z)\right]\,\mathcal{F} \tag{5}$$

where $\mathcal{A} = n_{\mathrm{el}}\,(N_{\mathrm{A}}/A_i)\,\epsilon\,\Omega/(4\pi)\,\omega_i\,p_i\,\sigma_i(E)\,(1+T_{CK})$ and $\chi_i = (\mu/\rho)_i\csc\theta$ is the X-ray attenuation factor.

In order to obtain the concentration c_i from the measured intensity I_i, as given by Eq. (5), measurements of the X-ray intensity are also performed on a reference standard that contains the element of interest. The ratio of intensities or k-ratio is given by:

$$K_i = \frac{I_i}{I_i^*} = \frac{c_i}{c_i^*}\,\frac{\displaystyle\int_0^{\infty}\Phi_i(\rho z)\;\exp\left(-\chi_i\,\rho z\right)\;\mathrm{d}(\rho z)}{\displaystyle\int_0^{\infty}\Phi_i^*(\rho z)\;\exp\left(-\chi_i^*\,\rho z\right)\;\mathrm{d}(\rho z)}\,\frac{\mathcal{F}}{\mathcal{F}^*} \tag{6}$$

where the superscript "*" indicates that the corresponding quantity is evaluated on the reference material. It is clear that, by using k-ratios, the factor A in Eq. (5) that contains instrumental and atomic parameters that are generally not well known cancel out. K-ratios are usually measured for the elements present in the sample and the resulting system of equations is solved by using an iterative procedure, since $\Phi(\rho z)$, μ/ρ and F also depend on the composition of the sample. In practice, simple analytical approximate expressions are used to parameterize the $\Phi(\rho z)$ function, which make it possible to estimate the elemental concentrations from measured k-ratios by means of relatively simple, algorithms [15].

Thin films on substrates and multilayers

Let us consider a thin film of mass thickness t deposited on a substrate. If the film is sufficiently thick, it can be possible to reduce the incident electron energy such that electrons do not penetrate the substrate. In this situation, we may treat the sample as if it were a bulk material (see [11] for additional considerations). If incident electrons penetrate the substrate, then the X-ray intensity emitted by the ith element in the film is given by:

$$I_{\mathrm{F}i} = \mathcal{A}\, c_i \left[\int_0^t \Phi_{\mathrm{F}i}(\rho z)\, \exp\left(-\chi_{\mathrm{F}i}\, \rho z\right)\, \mathrm{d}(\rho z)\right] \mathcal{F}_{\mathrm{F}} \tag{7}$$

where χ_{Fi} and $\Phi_{Fi}(\rho z)$ are the attenuation factor and depth-distribution of ionisations of element i in the film, respectively, and F_F is a fluorescence correction, which will now take into account fluorescence from X-rays generated both in the film and in the substrate. The X-ray intensity emitted by element j in the substrate is given by:

$$I_{\mathrm{S}j} = \mathcal{A}\, c_j\, \exp\left[(\chi_{\mathrm{S}j} - \chi_{\mathrm{F}j})\, t\right] \left[\int_t^\infty \Phi_{\mathrm{S}i}(\rho z)\, \exp\left(-\chi_{\mathrm{S}j}\, \rho z\right) \mathrm{d}(\rho z)\right] \mathcal{F}_{\mathrm{S}} \tag{8}$$

where χ_{Sj} and $\Phi_{Sj}(\rho z)$ are the attenuation factor and depth distribution of ionisations of element j in the substrate, respectively, and F_S is the corresponding fluorescence correction. The exponential outside the integral describes the attenuation of emitted X-rays in the overlayer. Notice that the integration interval now extends from t to infinity. When the target consists of several layers of different materials, the X-ray intensity emitted by the ith element of the kth layer, which extends from mass depth t_k to t_{k+1}, is given by:

$$I_{ki} = \mathcal{A}\, c_i \prod_{j=1}^{k-1} \exp\left[-(\chi_{ki} - \chi_{ji})\, T_j\right] \left[\int_{t_k}^{t_{k+1}} \Phi_{ki}(\rho z)\, \exp\left(-\chi_{ki}\, \rho z\right)\, \mathrm{d}(\rho z)\right] \mathcal{F}_k \tag{9}$$

where T_j is the mass thickness of layer j, χ_{ki} and $\Phi_{ki}(\rho z)$ are the attenuation factor and depth-distribution of ionisations of element i in the layer k and F_k is the corresponding fluorescence correction.

As for bulk samples, k-ratios are measured for the elements present in the thin film sample. However, the system of resulting equations is now more difficult to solve because there are additional variables (the thicknesses of the various layers) and also because some elements can be simultaneously present in different layers. To overcome these difficulties, k-ratio measurements are generally performed at two or more electron incident energies and the resulting system of equations, which is now over determined, is solved by using iterative methods. By doing so, values of the layer compositions and thicknesses that yield k-ratios that best match the experimental measurements are obtained.

For complex multilayers, convergence to the correct solution is not guaranteed, especially if the layer elements are not completely known or X-rays emitted from buried layers do not come out to the surface due to strong attenuation. Moreover, different combinations of element concentrations and layer thicknesses may lead to identical k-ratio curves vs. incident electron energies. In these cases, the number of equations can be increased by using more X-ray lines and electron incident energies and educated guesses of the film thicknesses and compositions are required. In other cases, data processing by a trial and error approach may be useful to provide the best fit to the experimental data. Nevertheless, in extreme situations, the determination of the composition and thickness of a complex multilayer film may become practically impossible by using only EPMA.

The Φ(ρz) function for thin films and multilayers

The depth-distribution of ionisations in thin films can deviate markedly from that in homogeneous samples, especially when the atomic numbers of film and substrate differ considerably. This effect is illustrated in Fig. 1, where results of MC simulation of the depth-distribution of ionisation for Al films of different thickness deposited on substrates of increasing atomic number are displayed. The distributions were obtained by means of the general-purpose MC code PENELOPE [17, 16]. We see that, in general, the number of ionisations increases with the atomic number of the substrate. Evidently, this fact is direct consequence of the stronger backscattering in heavier elements. We also see that differences between the ionisation distribution for the film and bulk material are larger at the interface, where the influence of the substrate is stronger, and it decreases as we move towards the sample surface. For relatively thin films, the influence of the substrate also reaches the surface and thus the surface ionisation also increases when the substrate atomic number increases. For films of intermediate thickness, the point of maximum ionisation gradually shifts to larger depths. Finally, for relatively thick films, backscattered electrons from the substrate are absorbed in the film before reaching the surface; in these cases, the surface ionisation does not vary with the substrate atomic number. For multilayer films, the modifications of the $\Phi(\rho z)$ function for an immersed layer are more complicated, because they stem from the combined effect of overlayers and underlayers [16].

THE X-FILM MODEL

In this section, we describe one of the thin-film programmes that is available at present, *X-FILM* [10], which was developed by one of us (C. Merlet). The programme *X-FILM* is based on a parameterisation of the $\Phi(\rho z)$ function as a double-Gaussian distribution. This analytical form is characterized by four parameters, namely the surface value $\Phi(0)$, the maximum value Φ_m, and the mass depths at which the distribution is maximum and zero, referred to as ρz_m and ρz_x, respectively. The double-Gaussian function can be written as the sum of two branches Φ_1 and Φ_2, with:

$$\begin{aligned} \Phi_1 &= \Phi_\mathrm{m} \exp\left[-\left(\rho z - \rho z_\mathrm{m}\right)^2/\beta^2\right] \quad \text{for } 0 < \rho z < \rho z_\mathrm{m} \\ \Phi_2 &= \Phi_\mathrm{m} \exp\left[-\left(\rho z - \rho z_\mathrm{m}\right)^2/\alpha^2\right] \quad \text{for } \rho z_\mathrm{m} < \rho z < \rho z_\mathrm{x} \end{aligned} \tag{10}$$

where:

$$\alpha = 0.46598\,(\rho z_\mathrm{x} - \rho z_\mathrm{m}) \quad \text{and} \quad \beta = \rho z_\mathrm{m}\,\frac{\ln(\Phi_\mathrm{m})}{\sqrt{\Phi(0)}} \tag{11}$$

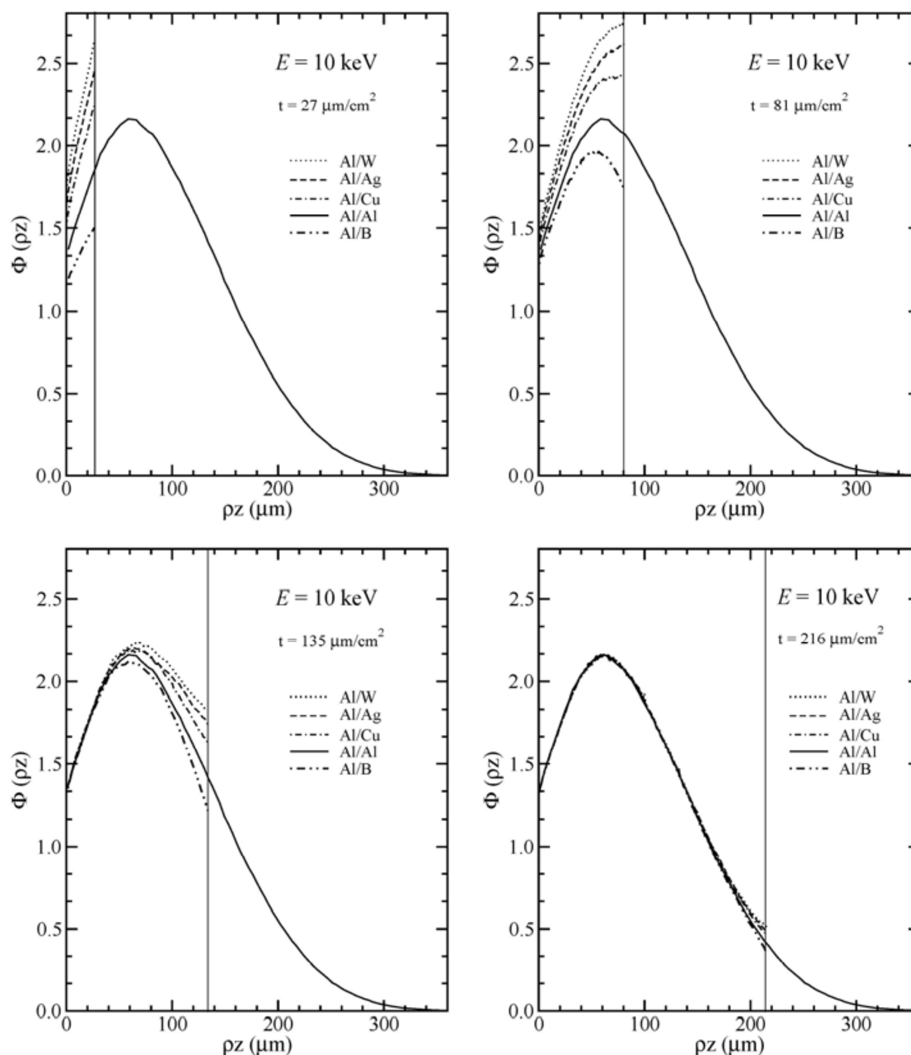

Fig. 1. Simulated depth distribution of ionisation for 10 keV electrons incident on Al films deposited on B, Al, Cu, Ag and W substrates. Lines are the results of MC simulation using PENELOPE.

Analytical expressions for the parameters $\Phi(0)$, Φ_m, ρz_m and ρz_x are given in Refs. [18, 20] for single- and multi-element bulk samples. The capability of the double-Gaussian function to reproduce experimental measurements of the $\Phi(\rho z)$ function is illustrated in Fig. 2, which compares measurements and calculations of the $\Phi(\rho z)$ function for Al Kα X-rays in Cu, for incident electrons of 20 keV. The experimental data are taken from Ref. [19]. The agreement between the measurements and the predictions of Merlet's model [18] is worth noting.

For thin films on substrates, *X-FILM* assumes that the depth-distributions of ionisations for the film-substrate combination can be described by a "weighted" average of that of bulk samples of the film and substrate materials. The weighting procedure implemented in *X-FILM*

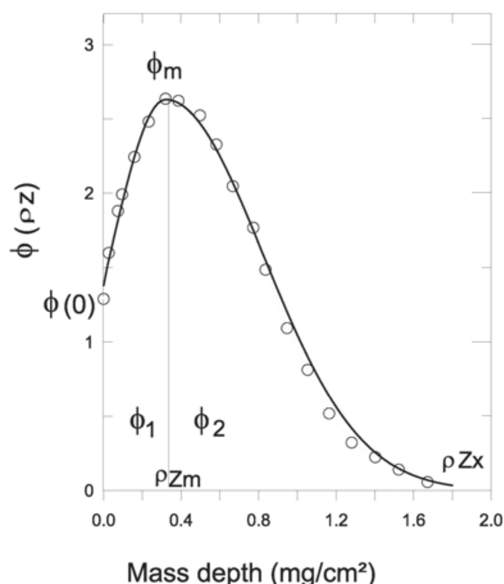

Fig. 2. Depth-distribution of ionisations for Al Kα in a Cu matrix. The continuous line is the prediction of the double-Gaussian model [18]. Symbols represent the experimental data of Castaing and Henoc [19].

is that proposed by Hunger and Rogaschewski [21] to describe the backscattering coefficient for thin films on substrates. This is applied to the parameters $\Phi(0)$, Φ_m, ρz_m and ρz_x, (denoted hereafter f for simplicity) and it is given by [10]:

$$f_{\mathrm{F/S}} = f_{\mathrm{S}} + (f_{\mathrm{F}} - f_{\mathrm{S}})\ \tanh\left(a_1 x + a_2 x^2\right) \tag{12}$$

where $f_{\mathrm{F/S}}$ stands for the $\Phi(\rho z)$ parameters of the film/substrate combination, f_{F} and f_S are those corresponding to bulk samples of the film and substrate materials, a_1 and a_2 are two parameters that depend on the film and substrate materials and x is a reduced thickness defined as $x = 4t/\rho z_x$. Expressions for a_1 and a_2 as functions of the mean atomic number of the film and substrate materials are given in Ref. [21]. In the case of a multilayer system, the parameters f are calculated iteratively starting from a fictitious sample consisting of the innermost layer and the substrate, and continuing until the outermost layer is reached [22]. Fig. 3 compares experimental values of the $\Phi(0)$ parameter for Ni Kα X-rays emitted from the surface of a 56 nm Cu/117-nm Bi/C multilayer film, with the predictions of *X-FILM* and the MC simulation code PENELOPE [22]. The agreement between the results of calculations, experiment and simulations is quite satisfactory, in spite of the uncertainties of such measurements (see also Ref. [23]). This example shows that simple, empirical weighting rules such as that defined by Eq. (12) can be successfully applied to describe the $\Phi(\rho z)$ parameters from multilayer films, even when they consist of relatively thick, adjacent layers with large differences in atomic number.

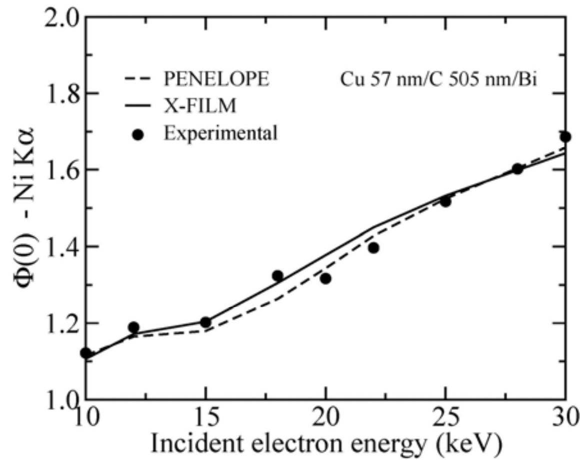

Fig. 3. Surface ionisation (Ni Kα) for a Cu 57 nm / C 505 nm / Bi multilayer film as functions of the electron incident energy. Dashed lines are MC simulation results using PENELOPE [17]; solid lines are the results from *X-FILM* [10]. Symbols are experimental data [22].

Using *X-FILM*, the X-ray intensity emitted by atoms of the *i*th element present in the *k*th layer, situated at a mass depth between t_k and t_{k+1}, is given by:

$$I_{ki} = \frac{\mathcal{A}\, c_i \Phi_m \zeta \sqrt{\pi}}{2} \exp(b) \prod_{j=1}^{k-1} \exp\left[-(\chi_{ki} - \chi_{ji})\, T_j\right] \left[\operatorname{erf}\left(\frac{t_{k+1}-\delta}{\zeta}\right) - \operatorname{erf}\left(\frac{t_k-\delta}{\zeta}\right)\right] \quad (13)$$

where χ_{ki} and χ_{ji} are attenuation factors of element *i* in layers *k* and *j*, "erf" is the error function, and

$$b = [(\zeta\ \chi_{ki})/2]^2 - \rho z_{\mathrm{m}} \chi_{ki} \quad \text{and} \quad \delta = \rho z_{\mathrm{m}} - (\zeta\ \chi_{ki})/2 \quad (14)$$

where:

$$\zeta = \begin{cases} \alpha & \text{for } 0 < \rho z < \rho z_{\mathrm{m}} \\ \beta & \text{for } \rho z_{\mathrm{m}} < \rho z < \rho z_{\mathrm{x}} \end{cases} \quad (15)$$

with α and β given by Eqs. (11). From Eqs. (13), (14) and (15), the calculation of the k-ratio is straightforward.

A large number of k-ratio measurements on well characterized thin film samples are available in the literature (e.g. [24 - 26]). As mentioned above, the k-ratio relates two

quantities given by integrals of the $\Phi(\rho z)$ function, which include a correction to take into account X-ray attenuation. Therefore, from the mere agreement between calculations and experiment we cannot conclude that the calculated $\Phi(\rho z)$ functions are correct to the same extent as the k-ratios. Nevertheless, these measurements are useful to validate the different thin-film programmes that have been proposed. As an example, Fig. 4 displays a comparison of the experimental measurements of Reuter et al. [24] for Al films on Si substrates, with the predictions of *X-FILM*. For the thickness values measured by these authors, the predictions of *X-FILM* are in good agreement with the experimental data.

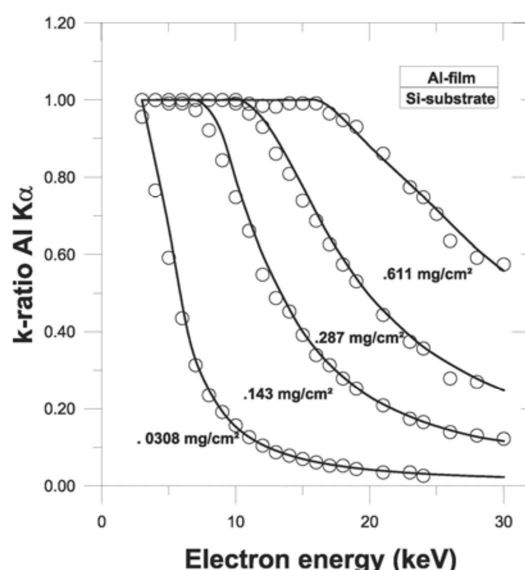

Fig. 4. K-ratios for Al films of several thicknesses deposited on Si substrates versus electron energy. Symbols are the measurements of Reuter et al. [24]; solid lines are the predictions of *X-FILM*.

EXAMPLES OF APPLICATIONS

In this section, we show some examples of thin-film analysis by EPMA which illustrate the capabilities of the technique. All the experimental data reported below were measured using a Cameca SX-100 electron microprobe. It is worth mentioning that EPMA of thin films can be carried out using the wavelength-dispersive spectrometer (WDS) as well as the energy-dispersive spectrometer (EDS). However, the use of WDS is generally preferred because of its higher peak-to-background ratio. Actually, the analysis of thin films faces similar experimental problems to those encountered in the analysis of trace and light elements in bulk samples [11]. Notice that the film density has to be known in order to estimate the linear thickness, as only the mass thickness can be determined by EPMA. A large number of examples of thin-film analysis by EPMA are available from publications (e.g. [11 - 14]).

Our first example corresponds to a very thin film of Au deposited on Ta. The goal of this study was to obtain the thickness of the film so as to determine the Au Mα X-ray production cross section [27]. As the thickness of the film was known to be very small (less than say 10 nm), the Au and Ta Mα lines were used for the measurements. Fig. 5 shows the k-ratio for the Au and Ta Mα lines as functions of the electron incident energy. K-ratios were measured from 4 keV to 30 keV in steps of 1 keV, using pure Au and Ta reference samples. The agreement between the experimental measurements and the predictions of *X-FILM*, for a thickness of 0.3 nm (assuming ρ = 19.32 g/cm^2) is excellent over all measured energies, for both the Au and Ta lines. The optimal choice of operating conditions (e.g. accelerating voltage and X-ray lines) is strongly dependent on the film thickness. In general, for increasing accelerating voltages (i.e. increasing beam penetration), the k-ratio becomes less sensitive to the thickness variation. In this example, the optimal range of accelerating voltages is seen to be from 4 to 10 keV. When the substrate and film composition are known, one k-ratio measurement at a single accelerating voltage can be sufficient to obtain the film thickness, however, owing to the smallness of the film thickness, a large number of k-ratio measurements were performed so as to minimize the influence of measurement errors on the resulting thickness. Measurement of k-ratios at a large number of incident electron energies is also useful to check the consistency of results and estimate their accuracy. In this case, the accuracy of thickness determination was quoted to be better than 5 %, partly because the atomic numbers of layer and substrate were close. This example shows the high sensitivity of EPMA for detecting near-surface layers.

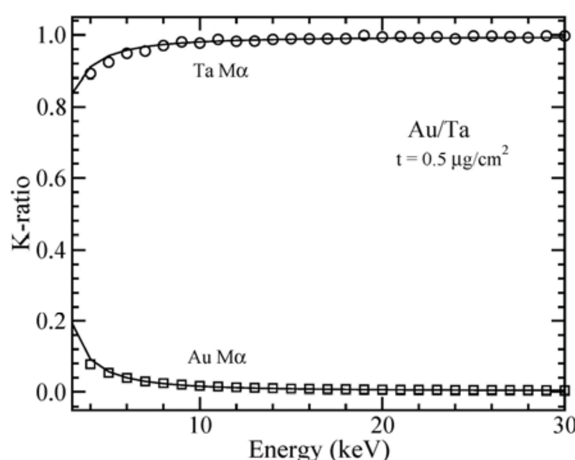

Fig. 5. K-ratios for the Au and Ta Mα lines emitted from a 0.25-nm thick Au/Ta film, as functions of the incident electron energy. The k-ratios were determined with respect to pure Au and Ta reference samples. Symbols represent experimental data. Curves are the predictions of *X-FILM* [10].

A second example illustrates the simultaneous determination of film thickness and composition. In this case, the sample is a Ga-As film deposited on Ni, which was used to obtain the K- and L-shell ionisation cross-sections of Ga and As [28]. K-ratios were measured for the Lα lines of Ni, Ga and As for electron incident energies from 10 to 39 keV, with respect to pure GaAs and Ni reference samples. The Kα lines of Ga and As were also measured to check the internal consistency of *X-FILM*, in an attempt to ensure that the film composition was uniform in depth and that the interface film-substrate was not affected by any oxidation or diffusion process. Fig. 6 compares measured k-ratios for the mentioned elements, lines and incident electron energies with the results of the best fit obtained with *X-FILM*, which gave a thickness of 5.6 nm (assuming ρ = 5.32 g/cm^2), and a composition of 62 at% Ga and 38 at% As. The agreement between the k-ratios measured and the *X-FILM* predictions over almost all the electron incident energies and analyzed lines is noticeable.

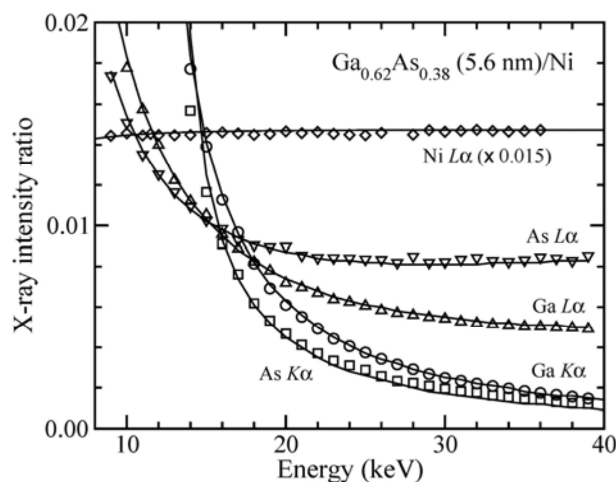

Fig. 6. K-ratios for the Ga Lα, As Lα, Ga Kα, As Kα, and Ni Lα lines emitted from a $Ga_{0.62}As_{0.38}$(5.6 nm) / Ni sample, as functions of the incident electron. Symbols represent experimental data. Curves are results from *X-FILM* [10].

The example of Fig. 7 concerns the determination of the thickness of a C film deposited on a Ag substrate. In this case, the difference in atomic numbers of the film and the substrate is larger than in previous examples; the C film was also known to be moderately thick. With this information, measurements were performed for the Ag Lα and C Kα lines, for incident electron energies between 2 and 25 keV. Fig. 7 shows the variation of C Kα and Ag Lα k-ratios versus incident electron energy and the best fit obtained with *X-FILM*, which gave a thickness value of 137 nm (assuming ρ = 2.2 g/cm^2). The agreement between calculated and experimental k-ratios is again satisfactory. During measurements, a liquid nitrogen cold stage was used so as to minimize carbon contamination. An additional problem found when working at low incident electron energies is that the presence of a native oxide layer at the surface (in

both samples and standards) may largely affect the accuracy of measured k-ratios. In these situations, thin-film programmes can also be used to correct measured k-ratios.

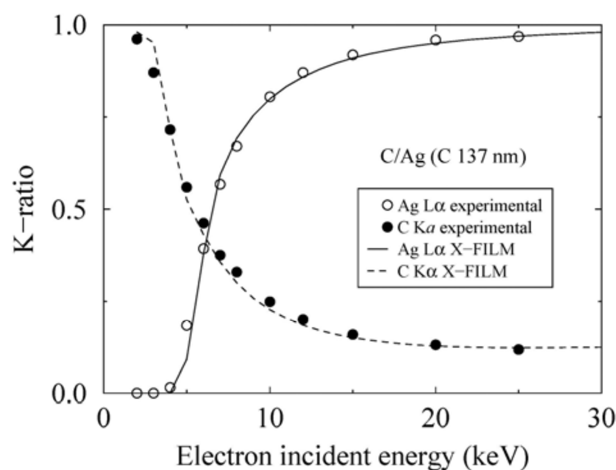

Fig. 7. Comparison between calculated and measured k-ratios for C Kα and Ag Lα from a 137 nm thick C film on Ag. Symbols represent experimental data. Continuous lines are results from *X-FILM*.

Our last example concerns the determination of the layer thickness of a Ni/Cu/C/Ag multilayer film. This sample was used for measuring the surface ionisation of multilayer films in unfavourable conditions, i.e. strong Z variation of adjacent layers [22]. The different layer elements and their situation in the multilayer were known. Measurements of the Lα lines of Ni, Cu and Ag, and the Kα lines of Cu and C were performed for incident electron energies between 4 and 30 keV. Fig. 8 shows a comparison of measured k-ratios and the best fit obtained with *X-FILM*, which gave the following result: Ni 5.6 nm / Cu 66 nm / C 1,013 nm / Ag (assuming ρ = 8.90 g/cm^2 for Ni, ρ = 8.96 g/cm^2 for Cu and ρ = 2.22 g/cm^2 for C). In this case, the agreement between the predictions of *X-FILM* and the experimental data is not as good as previous examples, although it can be considered to be satisfactory owing to the complexity of this sample.

ACKNOWLEDEGEMENTS

The authors wish to thank F. Salvat for helpful discussions and for critically reading the manuscript.

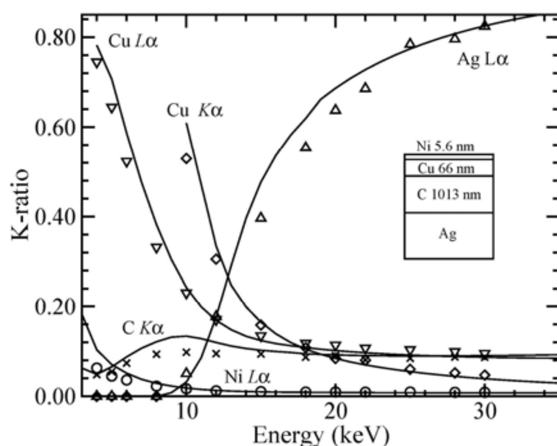

Fig. 8. Comparison between calculated and measured k-ratios for a multilayer sample of the type Ni (5.6 nm) / Cu (66 nm) / C (1013 nm) / Ag. Symbols represent experimental data. Continuous lines are results from *X-FILM*.

REFERENCES

[1] S.J.B. Reed (1993) *Electron Microprobe Analysis*. Cambridge University Press.

[2] A.P. Mackenzie (1993) *Rep. Prog. Phys.*, **56**, 557.

[3] R. Castaing (1951) Ph.D. Thesis, University of Paris. Publication ONERA No. 55,

[4] H.J. Hunger (1988) *Scanning*, **10**, 65.

[5] D.F. Kyser and K. Murata (1974) *IBM J. Res. Dev.*, **18**, 352.

[6] J.L. Pouchou and F. Pichoir (1984) *Rech. Aerosp.*, **5**, 47.

[7] R. Waldo (1988) in: "*Microbeam Analysis*" (D. Newbury, Ed.). San Francisco Press, 310.

[8] R.H. Packwood and G. Remond (1992) *Scanning Microsc.*, **6**, 367.

[9] G.F. Bastin, J.M. Dijkstra, H.J.M. Heijligers and D. Klepper (1993) *Microbeam Anal.*, **2**, 29.

[10] C. Merlet (1995) in: "*Proc. Microbeam Analysis*" (E.S. Etz, Ed.) VHC Publishers, 203.

[11] P. Willich (1992) *Mikrochim. Acta*, **Suppl. 12**, 1.

[12] J.L. Pouchou and F. Pichoir (1993) *Scanning Microsc.*, **Suppl. 7**, 167.

[13] J.L. Pouchou (2002) *Mikrochim. Acta*, **138**, 133.

[14] G.F. Bastin (2006) in: "*Electron Probe Microanalysis Today. Practical Aspects*" 7th EMAS Regional Workshop, Book of Abstracts, 33.

[15] K.F.J. Heinrich and D.E. Newbury (Eds.) (1991) *Electron Probe Quantitation*. Plenum Press.

[16] X. Llovet (1998) Ph.D. Thesis, University of Barcelona.

[17] F. Salvat, J.M. Fern´andez-Varea and J. Sempau (2006) *PENELOPE. A code system for Monte Carlo simulation of Electron and Photon Transport*. OECD/NEA Data Bank:Issy-les-Moulineaux (France).

[18] C. Merlet (1992) *Mikrochim. Acta*, **Suppl. 12**, 107.

[19] R. Castaing and J. Henoc (1965) in: "*Optique des Rayons X et Microanalyse, 4th Congres*" (R. Castaing, P. Descamps and J. Philibert, Eds.). Hermann.

[20] C. Merlet (1994) *Mikrochim. Acta*, **114/115**, 363.

[21] H.J. Hunger and S. Rogaschewski (1986) *Scanning*, **8**, 257.

[22] C. Merlet, X. Llovet and F. Salvat (2004) *X-Ray Spectrom.*, **33**, 376.

[23] X. Llovet, C. Merlet and F. Salvat (1998) *Mikrochim. Acta*, **Suppl. 15**, 155.

[24] W. Reuter, J.D. Kuptsis, A. Lurio and D.F. Kyser (1978) *J. Phys. D: Appl. Phys.*, **11**, 2633.

[25] G.F. Bastin and H.J.M. Heijligers (2000) *X-Ray Spectrom.*, **29**, 212.

[26] G.F. Bastin and H.J.M. Heijligers (2000) *X-Ray Spectrom.*, **29**, 373.

[27] C. Merlet, X. Llovet and F. Salvat (2008) *Phys. Rev. A*, submitted.

[28] C. Merlet, X. Llovet and J.M. Fern´andez-Varea (2006) *Phys. Rev. A*, **73**, 062719.